# Synthesis and study of the heavy-fermion compound $Yb_5Pt_9$

M. S. Kim,[1] M. C. Bennett,[1] D. A. Sokolov,[1] M. C. Aronson,[1] J. N. Millican,[2] Julia Y. Chan,[2] Q. Huang,[3] Y. Chen,[3,4] and J. W. Lynn[3]

[1]*Department of Physics, University of Michigan, Ann Arbor, Michigan 48109-1120, USA*

[2]*Department of Chemistry, Louisiana State University, Baton Rouge, Louisiana 70803, USA*

[3]*NIST Center for Neutron Research, NIST, Gaithersburg, Maryland 20899, USA*

[4]*Department of Materials Science and Engineering, University of Maryland, College Park, Maryland 20742, USA*

(Received 29 June 2006; revised manuscript received 28 September 2006; published 26 December 2006)

We report the synthesis of single crystals of a binary heavy-fermion system $Yb_5Pt_9$. An unusual double phase transition is observed in specific heat $C_P$ measurements at 0.6 K and 0.65 K, signaling a magnetically ordered ground state. The complete magnetic field-temperature phase diagram of $Yb_5Pt_9$ is obtained from the magnetic field dependence of the electrical resistivity $\rho(T)$ and specific heat $C_P(T)$, and consists of two phase lines terminating at finite temperature critical endpoints. Electrical resistivity and specific heat measurements show that the magnetically ordered state is a Fermi liquid with strong electronic correlations, absent in the paramagnetic state. At higher temperatures, strong magnetic anisotropy is observed, which we ascribe to crystal electric field effects acting on a well localized $Yb^{3+}$ moment, yielding a well separated doublet ground state, confirmed by inelastic neutron scattering measurements. Our measurements show that $Yb_5Pt_9$ is a heavy-fermion compound which is very near a quantum critical point.

DOI: 10.1103/PhysRevB.74.224431 PACS number(s): 75.30.Mb, 75.20.Hr, 71.27.+a

## I. INTRODUCTION

Heavy-fermion systems based on Ce and U intermetallic compounds have attracted much attention, because the competition between the intrasite Kondo screening and the intersite exchange interaction induces many interesting phenomena, especially quantum critical points and their associated non-Fermi-liquid behaviors.[1,2] Recently, unconventional superconductivity was found in the ferromagnetic heavy fermion compounds $UGe_2$ and URhGe.[3,4] These discoveries have renewed interest in finding heavy-fermion compounds which order ferromagnetically, particularly those with quantum critical points where superconductivity may compete or coexist with types of magnetic order. Although the Ruderman-Kittel-Kasuya-Yosida (RKKY) interaction which is responsible for magnetic order in heavy-fermion compounds enables both ferromagnetic and antiferromagnetic order, heavy-fermion compounds with ferromagnetic ordering are rarely reported. Thus, the discovery of ferromagnetic heavy fermion compounds is important due to the richness of the physics, particularly near ferromagnetic quantum critical points.[5]

The electronic configuration of $f^{13}$ for Yb can be considered the hole analogue to the $f^1$ electronic configuration of Ce, suggesting that the same phenomena can be realized in Yb-based compounds. However, much less experimental attention has focused on Yb-based compounds, because the synthesis of Yb-intermetallic compounds is difficult due to the high vapor pressure of Yb. Most of the Yb-based Kondo lattice systems investigated so far order antiferromagnetically,[6–9] but several have been found to order at least partly ferromagnetically.[10–12] We report here the synthesis of a Yb-based intermetallic compound, $Yb_5Pt_9$, and present the results of transport, magnetic, and thermal properties.

## II. EXPERIMENTAL DETAILS

Single-crystalline samples of $Yb_5Pt_9$ were grown using a Pb flux. The single crystals are hexagonal prisms with typical dimensions of $0.5\times0.5\times1$ mm.[3] Electron-probe microanalysis was carried out on polished single crystals using a Cameca SX100 microprobe system with elemental Yb and Pt standards. The 5:9 atomic ratio of Yb:Pt is uniform within a systematic error of 2% over the whole crystal surface. Indeed, the electron backscattering image indicates homogeneous composition without surface phases or inclusions. Several other Yb-Pt binary compounds have been reported[14–20] and their magnetic properties described,[21–23] but $Yb_5Pt_9$ has not previously been reported. Single crystal x-ray diffraction measurements indicate that $Yb_5Pt_9$ crystallizes in an orthorhombic *Cmmm* (No. 65) space group with lattice parameters of $a=13.5550(5)$, $b=13.3720(5)$, $c=5.6540(3)$ Å, and $V=1024.83(8)$ Å$^3$, with $Z=19$. The structure was solved and refined using the SHELXL-97 program.[24] Corrections were made for absorption and extinction, and the atomic positions were refined with anisotropic displacement parameters. Atomic coordinates and thermal parameters are listed in Table I, and a schematic representation of the unit cell of $Yb_5Pt_9$ is shown in Fig. 1. Laue x-ray diffraction revealed that the orthorhombic $c$ axis is along the prism axis of the crystal.

The electrical resistivity was measured by the conventional four-probe method between 0.4 and 300 K in zero field and in magnetic fields as large as 0.1 T. Magnetization and magnetic susceptibility were measured using a quantum design magnetic property measurement system in magnetic fields up to 7 T. Specific heat measurements were performed using a quantum design physical property measurement system for temperatures between 0.4 and 70 K. Inelastic neutron scattering measurements were performed on a sample prepared by powdering four grams of $Yb_5Pt_9$ single crystals.

 

TABLE I. Crystallographic data for $Yb_5Pt_9$.

| Atom | Site | $x$ | $y$ | $z$ | $U_{eq}$ (Å$^2$)[a] |
|---|---|---|---|---|---|
| $Yb_1$ | 2*b* | 1/2 | 0 | 0 | 0.0071(10) |
| $Yb_2$ | 2*d* | 1/2 | 1/2 | 1/2 | 0.0060(8) |
| $Yb_3$ | 8*p* | 0.32260(14) | 0.63083(19) | 0 | 0.0062(7) |
| $Yb_4$ | 8*q* | 0.36889(15) | 0.82253(15) | 1/2 | 0.0043(7) |
| $Pt_1$ | 2*a* | 1/2 | 1/2 | 0 | 0.0060(8) |
| $Pt_2$ | 2*c* | 1/2 | 0 | 1/2 | 0.0071(9) |
| $Pt_3$ | 8*n* | 1/2 | 0.69230(16) | 0.7502(2) | 0.0037(7) |
| $Pt_4$ | 8*o* | 0.30769(13) | 0 | 0.7499(2) | 0.0033(7) |
| $Pt_5$ | 8*p* | 0.38884(12) | 0.83037(14) | 0 | 0.0041(6) |
| $Pt_6$ | 8*q* | 0.33043(11) | 0.61154(15) | 1/2 | 0.0046(7) |

[a]$U_{eq}$ is defined as one-third of the trace of the orthogonalized $U_{ij}$ tensor.

These experiments were performed at the NIST Center for Neutron Research using the BT-7 double focusing triple-axis spectrometer with a fixed final energy of 14.7 meV, and at several fixed wave vectors. We used the double focusing PG monochrometer, and focusing analyzer to get the maximum intensity. Neutron diffraction measurements were carried out on the identical powder sample using the BT-1 powder diffractometer at NIST, equipped with a Ge 311 vertically focusing monochrometer, at a neutron wavelength of 2.079 Å.

## III. RESULTS AND DISCUSSION

The temperature dependence of the electrical resistivity $\rho$ is metallic, as shown in the inset of Fig. 2(a). The room temperature value of $\rho$ is 35 $\mu\Omega$ cm. With decreasing temperature, $\rho$ decreases approximately linearly to about 25 K, suggesting that electron-phonon scattering dominates the resistivity, at least for temperatures above the Debye temperature, which we estimate is about 250 K. Increasing curvature is observed in $\rho(T)$ below 25 K, suggesting that magnetic scattering mechanisms are relatively more important at low temperatures. As shown in Fig. 2(a), $\rho$ is nearly independent of temperature in the range between 2 and 25 K, although a

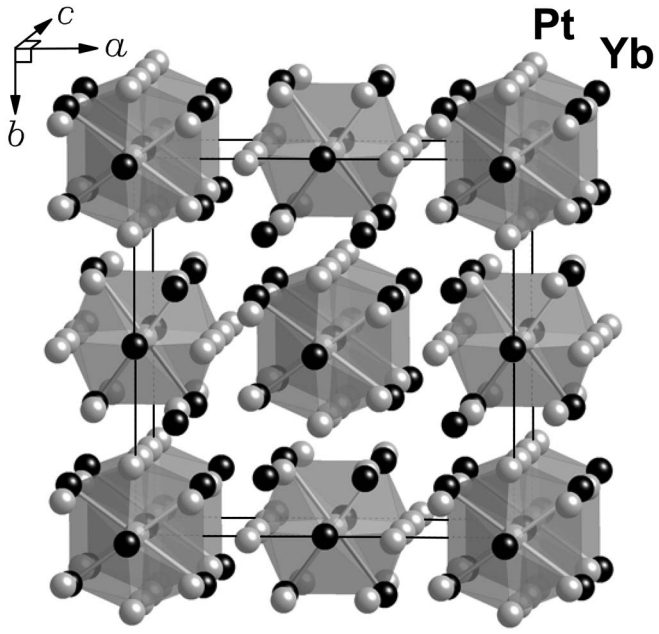


FIG. 1. Schematic representation of the unit cell of $Yb_5Pt_9$ crystallizing in an orthorhombic *Cmmm* (No. 65). There are 20 Yb atoms and 36 Pt atoms in the unit cell of $Yb_5Pt_9$.

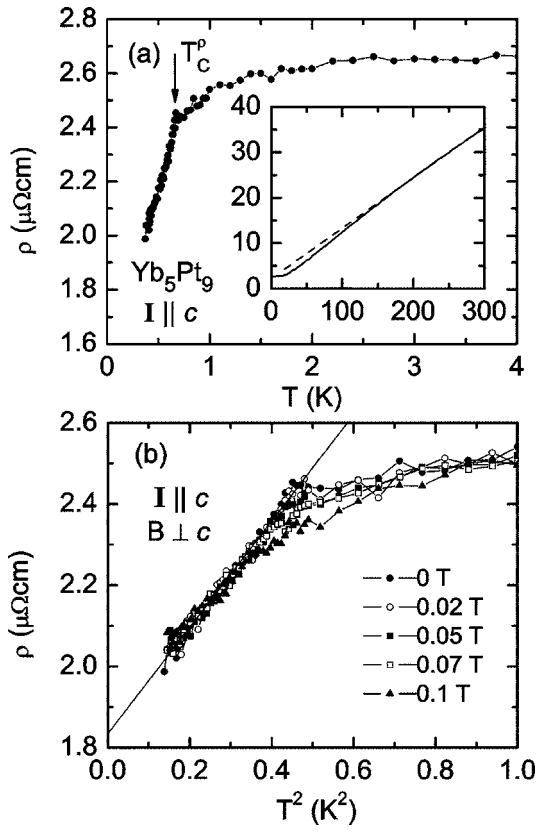


FIG. 2. (a) The temperature dependence of the electrical resistivity $\rho(T)$ for $Yb_5Pt_9$ below 4 K. The arrow indicates the magnetic phase transition at 0.66 K. The inset shows the resistivity over an expanded range of temperatures. (b) $\rho$ as a function of $T^2$ in magnetic fields of 0, 0.02, 0.05, 0.07, and 0.1 T. Solid line indicates fits to $\rho(T)=\rho_0+AT^2$.

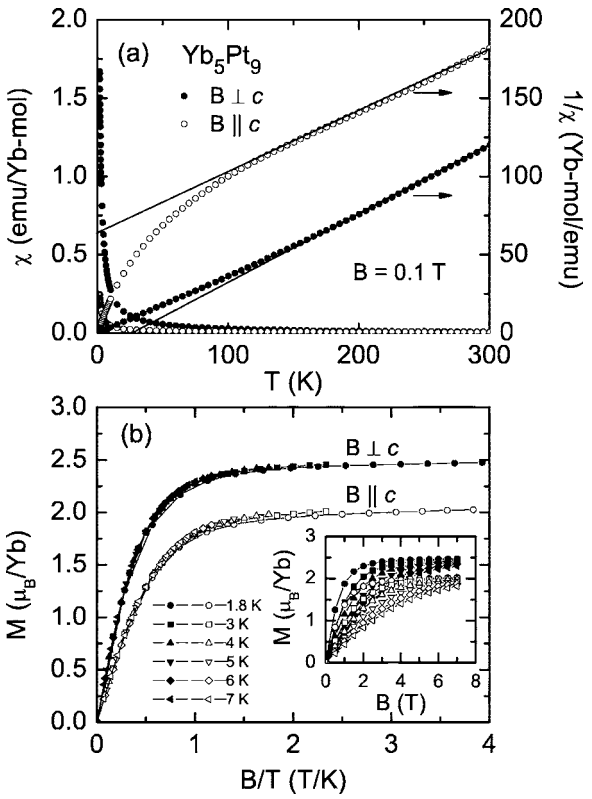


FIG. 3. (a) The temperature dependence of the magnetic susceptibility $\chi$ and inverse magnetic susceptibility $1/\chi$ in the magnetic field $B=0.1$ T parallel to the $c$ axis ($\chi_\parallel$) and perpendicular to the $c$ axis ($\chi_\perp$). (b) A plot of the magnetization $M$ vs $B/T$. The inset shows the magnetic field dependence of $M$ at low temperatures with fields as large as 7 T applied along both sample axes.

rounded decrease is observed below 2 K, perhaps due to partial Kondo compensation. A sharp drop is found at 0.66 K, marked with an arrow as a magnetic transition temperature ($T_C^\rho$). Figure 2(b) shows $\rho$ plotted as a function of $T^2$ below 1 K in magnetic fields of 0, 0.02, 0.05, 0.07, and 0.1 T. As the magnetic field increases, the transition temperature $T_C^\rho$ gradually decreases and a negative magnetoresistance is found above $T_C^\rho$, indicating that the magnetic transition is sensitive even to the weakest magnetic fields. Such a sharp drop and negative magnetoresistance is characteristic of the loss of spin disorder scattering found at a magnetic phase transition. In the low temperature ordered state $T \leqslant T_C^\rho$, we find that $\rho(T)$ is well described by the Fermi liquid expression $\rho(T)=\rho_0+AT^2$, with the residual resistivity $\rho_0=1.83$ $\mu\Omega$ cm. The low value of $\rho_0$ attests to the high quality and crystallinity of our samples. The coefficient $A$ is 1.31 $\mu\Omega$ cm/K$^2$, comparable with that found in the heavy fermion superconductor $UPt_3$ (=1.6 $\mu\Omega$ cm/K$^2$).[25] This suggests that the quasiparticles in the magnetically ordered state are strongly interacting.

Figure 3(a) shows the magnetic susceptibility $\chi(T)$ and the inverse magnetic susceptibility $1/\chi(T)$ of $Yb_5Pt_9$ with the measuring field of 0.1 T oriented along the $c$ axis ($\chi_\parallel$) and perpendicular to the $c$ axis ($\chi_\perp$). $\chi_\perp$ is 7 times larger than $\chi_\parallel$ at 1.8 K, indicating that the magnetization easy axis is perpendicular to the $c$ axis. With decreasing temperature, $1/\chi_\parallel$ decreases linearly down to 100 K and at lower temperatures deviates below the linear behavior. $1/\chi_\perp$ deviates above the linear extrapolation below 100 K. These strong departures from Curie-Weiss behavior can result from crystal electric field (CEF) effects, from the Kondo effect, and from precursor effects related to magnetic order. Considering the large magnetic anisotropy, we believe that CEF effects are particularly strong, resulting from the low crystal symmetry of the orthorhombic structure. As shown in Fig. 3, the magnetic susceptibility $\chi(T)$ is well described by the Curie-Weiss expression between 100 K and 300 K, for both field orientations. The Curie temperatures found from these fits are −149 and 27 K for $\chi_\parallel$ and $\chi_\perp$, respectively. The effective moments of 4.41 and 4.24$\mu_B$, respectively, are close to 4.54$\mu_B$ expected for free $Yb^{3+}$, indicating that the magnetic moments are well localized and trivalent at high temperatures. The inset of Fig. 3(b) shows the magnetization for fields up to 7 T applied along both crystal axes, for temperatures from 1.8 K to 7 K. A nonlinear curvature is observed which becomes increasingly pronounced at the lowest temperatures. At 1.8 K, the magnetic moment saturates above 2 T at the values of 2.0 and 2.5$\mu_B$ for fields parallel and perpendicular to the $c$ axis, respectively. While this saturation can be characteristic of incipient ferromagnetic order, Fig. 3(b) shows instead that the magnetization collapses onto a universal curve when the field is scaled by the absolute temperature. Further, the collapsed data are well described by a $S=1/2$ Brillouin function, which suggests that the curvature in the magnetization curves reflects normal paramagnetic behavior. We note that the saturation moments are much reduced from the fully degenerate value of 4.5$\mu_B$, but are consistent with values found in other Yb-based compounds with the orthorhombic structure.[6,9,10,12,13] This suggests that magnetic order in $Yb_5Pt_9$ arises from a doublet ground state caused by the orthorhombic CEF.

In order to determine the ground state and energy level scheme for the $Yb^{3+}$ moments, we have measured the specific heat $C_P$ of our sample for temperatures from 0.4 K to 70 K (Fig. 4). The magnetic part of the specific heat was isolated from $C_P$ by estimating the phonon contribution $C_{\rm ph}(T)$. $C_{\rm ph}(T)$ was calculated by fitting the high temperature $C_P$ by the Debye model. The Debye temperature, $\Theta_D=236$ K is extracted from the linear extrapolation of the plot of $C_P/T$ vs $T^2$ above 6 K, with the electronic specific heat coefficient $\gamma_h=15$ mJ/Yb mol K$^2$, as shown in the inset of Fig. 4. We note that the Debye temperature obtained from the specific heat data is in good agreement with the value of ~250 K deduced from the linear temperature dependence of resistivity above 150 K $\sim 0.6\Theta_D$ in the inset of Fig. 2(a). The magnetic part of the specific heat is presented on a logarithmic temperature scale in Fig. 4, displaying a sharp lambda-like anomaly near the magnetic phase transition at 0.66 K, and a gradual decrease at higher temperatures. The prominent tail of the heat capacity between $T_C$ and 2 K may be ascribed to the specific heat of an $S=1/2$ Kondo compensated moment, with a Kondo temperature $T_K$ of approximately 1 K.[26] The inset of Fig. 5 shows the electronic part of the specific heat in the ordered phase $C_{\rm el}=C_P-C_{\rm ph}=\gamma_1 T$, where the large value of $\gamma_1=355$ mJ/Yb mol K$^2$ reveals that magnetic order in $Yb_5Pt_9$ results in the formation of a Fermi

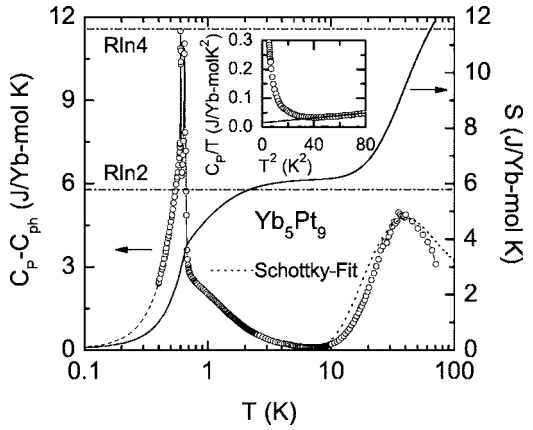


FIG. 4. The logarithmic temperature dependence of the specific heat $C_P$ from which we have subtracted an estimated phonon contribution $C_{\mathrm{ph}}$, and the associated entropy $S$. The dashed line indicates the interpolation of $(C_P - C_{\mathrm{ph}})/T$ vs $T^2$ below 0.4 K. The dotted line indicates a fit to a Schottky expression, yielding a peak at about 40 K. The inset represents the plot of $C_P/T$ vs $T^2$ from which the electronic part of the specific heat, $\gamma T$ is extracted.

liquid comprised of strongly interacting quasiparticles. Combining these results with those of the resistivity measurements, we find that $A/\gamma_1^2$ is $1.2 \times 10^{-5}$ $\mu\Omega$ cm $\mathrm{K}^{-2}/(\mathrm{mJ\ mol}^{-1}\ \mathrm{K}^{-2})^2$, very close to the value of $1.0 \times 10^{-5}$ $\mu\Omega$ cm $\mathrm{K}^{-2}/(\mathrm{mJ\ mol}^{-1}\ \mathrm{K}^{-2})^2$, known as the Kadowaki-Woods ratio, observed in many heavy-fermion systems.[27]

The temperature dependence of the entropy confirms the crystal field scenario which we proposed on the basis of magnetization measurements. The temperature dependence of the entropy $S$ was determined by integrating $C_{\mathrm{mag}}/T$, and is overplotted in Fig. 4. Just above the magnetic phase transition, $S = 0.65R \ln 2$ and gradually increases to $R \ln 2$ at 2 K. $S$ remains approximately constant until ~10 K, showing that magnetic order develops from a doublet ground state. Above 10 K, $S$ begins to increase again and finally attains the value $R \ln 4$ at 70 K. This is consistent with the observation of the Schottky anomaly at 40 K, and the fit to this anomaly shown in Fig. 4 finds that the splitting between the ground doublet and the first excited state, also a doublet, is ~70 K.

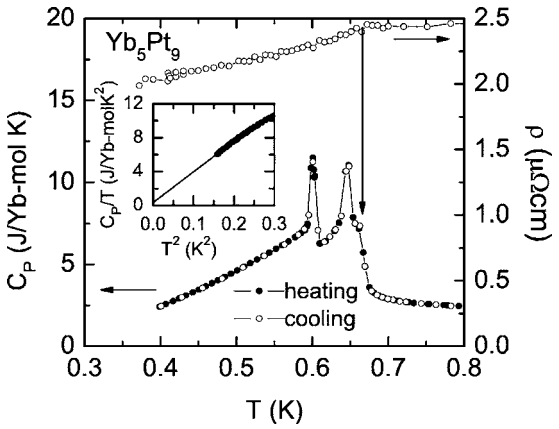


FIG. 5. The temperature dependence of the specific heat $C_P$ and electrical resistivity $\rho$ below 0.8 K.

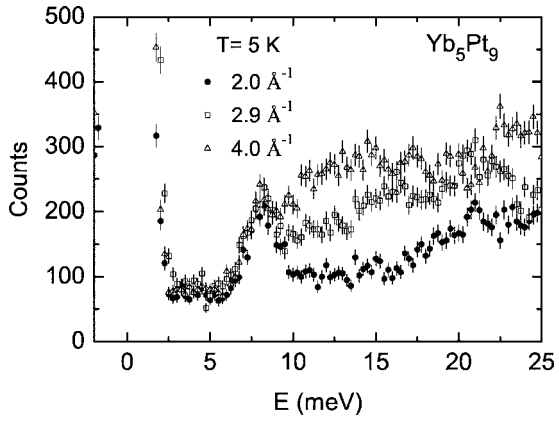


FIG. 6. Inelastic neutron scattering spectra at 5 K for wave vectors of 2, 2.9, and 4 $\mathrm{Å}^{-1}$. The first excited crystal field level is observed at 8.27(5) meV. The scattering extending to higher energies is dominated by the phonon density of states.

Direct evidence for the splitting of the ground and excited doublets comes from inelastic neutron scattering measurements, shown in Fig. 6. A sharp peak is observed at 8.27 meV, whose intensity decreases with wave vector in approximate agreement with the $Yb^{3+}$ magnetic form factor while the energy is approximately independent of wave vector, indicating that this is a crystal field excitation. The scattering at higher energies is found to increase in intensity with increasing wave vector suggesting that this scattering is predominantly lattice dynamical in origin. Data at a wave vector of 2 $\mathrm{Å}^{-1}$ were also collected at a series of temperatures from 5 K to 300 K. There is only a modest decrease in the intensity of this crystal field transition up to ~100 K, which indicates that this is the first crystal field excited state. At higher temperatures this peak decreases in intensity and broadens substantially, and is essentially unobservable at room temperature. The phonon scattering, which extends into the 8 meV range (and below), increases steadily with increasing $T$ as expected for the thermal population factor for bosons. We note that the splitting between the ground state and the first excited state deduced from heat capacity measurements (70 K) is in quite reasonable agreement with the direct measurement from inelastic neutron scattering measurements (8.3 meV, 96.4 K), validating our crystal field scheme.

The low temperature specific heat $C_P$, shown in Fig. 5, demonstrates that the magnetic phase transition in $Yb_5Pt_9$ is highly unconventional. The specific heat reaches a huge value of 12 J/Yb mol K, and consists of two large peaks at 0.6 K and 0.65 K, followed by a shoulder at 0.66 K, where a sharp drop is found in $\rho$. However, we see from Fig. 5 that $\rho$ has no anomaly at either of the temperatures where the specific heat displays maxima. The specific heat anomalies are not ideally lambda-like, but no hysteresis was found in the specific heat on cooling and heating, indicating that the phase transitions are at best weakly first order. We repeated these measurements on several other crystals from different preparation batches, and the results in Fig. 5 were exactly reproduced in each case.

Neutron diffraction experiments have been used to investigate the nature of the magnetic order at the 0.6 K and

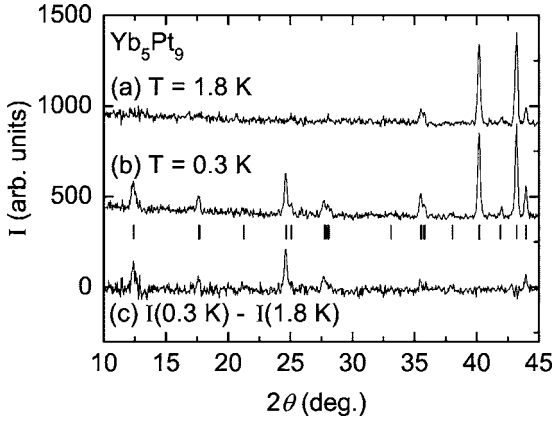


FIG. 7. A comparison of the neutron powder patterns for $Yb_5Pt_9$ at 1.8 K (a), 0.3 K (b), and their difference (c). All the peaks can be indexed in the crystal unit cell, indicating that the magnetic order is possibly ferromagnetic.

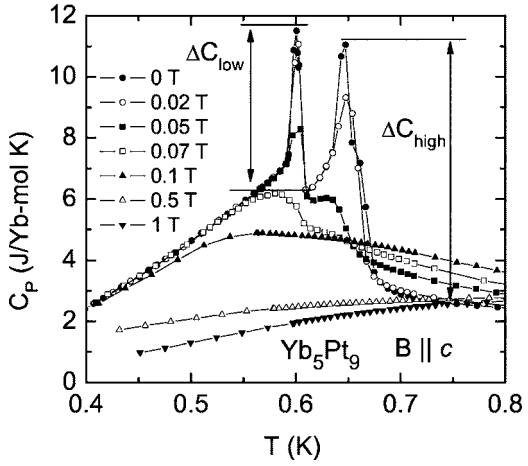


FIG. 8. The temperature dependence of the specific heat $C_P$ in magnetic fields as large as 1 T. $\Delta C_{\text{high}}$ and $\Delta C_{\text{low}}$ are the heat capacity steps at the higher and lower temperature phase transitions.

0.65 K phase transitions in $Yb_5Pt_9$. Figure 7 compares the powder pattern obtained at 1.8 K, where the sample is paramagnetic, to the powder pattern at 0.3 K, where the sample is magnetically ordered. We note that the 1.8 K powder pattern is in full agreement with the structure determined from single crystal x-ray diffraction. While the details of the magnetic structure will be presented elsewhere,[28] the magnetic ordering wave vector was found to be wholly commensurate, adding to the intensities of the nuclear Bragg peaks with reduced temperature. Every peak at 0.3 K can be indexed within the reported orthorhombic structure. There are two possible interpretations of this finding. One possibility is that the ground state is ferromagnetic, or alternatively, given that there are four inequivalent Yb atoms per unit cell, it is possible that the order is antiferromagnetic with a wave vector commensurate with the high temperature reciprocal lattice. While a definitive answer to this question awaits a determination of the magnetic structure,[28] the field dependence of the heat capacity suggests that the magnetic ground state has a ferromagnetic component.

As expected for ferromagnetic states, Fig. 8 shows that both peaks in the specific heat are strongly suppressed by magnetic field, with the upper transition being more sensitive to field than the lower transition. Above 0.05 T, the high temperature peak evolves into a rounded shoulder, and the low temperature peak is broadened and shifted to lower temperatures. A field of only 0.1 T is sufficient to totally suppress both peaks, yielding an extremely broad but still field dependent maximum. Above 0.1 T, both peaks merge into a single broad peak, whose intensity decreases and shifts to higher temperatures with increasing field. The magnetic field dependences of the two specific heat transition temperatures are plotted in Fig. 9. We have plotted the jumps $\Delta C$ in the specific heat at the two transitions in the inset of Fig. 9. The thermodynamic signatures of the magnetic phase transitions $\Delta C_{\text{high}}$ and $\Delta C_{\text{low}}$ go to zero at fields of 0.07 T for the upper transition, and 0.1 T for the lower temperature transition. It is remarkable that the transition temperatures themselves remain finite in these fields, suggesting that the phase lines reproduced in Fig. 9 terminate in critical endpoints.

## IV. CONCLUSION

We have reported here the synthesis of single crystals of $Yb_5Pt_9$, which we show is a heavy-fermion magnet. Paramagnetic behavior is found at high temperatures, involving the full $Yb^{3+}$ moment. With decreasing temperature, the moment degeneracy is lifted by the crystal electric field, resulting in strong magnetic anisotropy and a doublet ground state well separated from the excited doublet states. Magnetic order results in a low temperature Fermi liquid state, revealed by resistivity and specific heat measurements to have quasiparticle interactions as strong as those found in well-studied heavy-fermion compounds like $UPt_3$. Neutron diffraction measurements find that the ordering wave vector of the ground state is commensurate with the reciprocal lattice in the paramagnetic state. Specific heat measurements find an unusual magnetic ordering transition which proceeds by two

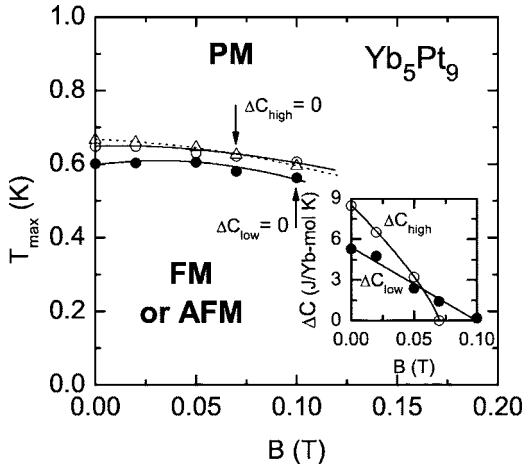


FIG. 9. The phase diagram of $Yb_5Pt_9$. $T_C^{\rho}$ (△) is the transition temperature found in $\rho(T,B)$ in Fig. 2(b), and $T_{\text{max}}^{\text{high}}$ (○) and $T_{\text{max}}^{\text{low}}$ (●) are the transition temperatures taken from the specific heat data (Fig. 8). The inset shows the magnetic field dependence of the height of two peaks, $\Delta C_{\text{high}}$ and $\Delta C_{\text{low}}$ at the high and low transition temperatures, respectively.

steps, the first at 0.65 K and an additional one at 0.6 K. We find that very modest magnetic fields are sufficient to suppress both magnetic ordering transitions to lower temperatures, while the specific heat anomaly at each transition disappears even more rapidly. The magnetic phase diagram thus consists of two magnetic phase lines, which are at best weakly first order, terminating at finite temperature and/or finite field critical endpoints. We conclude that while the ordering temperatures of $Yb_5Pt_9$ are quite low, this system effectively avoids the generation of a quantum critical point, where the critical endpoints are suppressed to zero temperature. This fact suggests that the typical signs of quantum criticality should be absent in this material, and indeed we find evidence for only conventional Fermi liquid phenomena in the magnetically ordered phase.

## ACKNOWLEDGMENTS

The authors are grateful to C. Henderson for assistance with the electron-probe microanalysis, which was performed at the University of Michigan Electron Microbeam Analysis Laboratory (EMAL). Work at the University of Michigan is supported by the National Science Foundation under Grant No. NSF-DMR-0405961. Work at Louisiana State University is supported by Grant No. NSF-DMR-0237664 and by the Alfred P. Sloan Foundation. Identification of commercial equipment in the text is not intended to imply recommendation or endorsement by the National Institute of Standards and Technology.

[1] S. Doniach, in *Valence Instabilities and Related Narraw Band Phenomena*, edited by R. D. Parks (Plenum, New York, 1977), p. 169.
[2] B. A. Jones, C. M. Varma, and J. W. Wilkins, Phys. Rev. Lett. **61**, 125 (1988).
[3] S. S. Saxena, P. Agarwal, K. Ahilan, F. M. Grosche, R. K. W. Haselwimmer, M. J. Steiner, E. Pugh, I. R. Walker, S. R. Julian, P. Monthoux, G. G. Lonzarich, A. Huxley, I. Sheikin, D. Braithwaite, and J. Flouquet, Nature (London) **406**, 587 (2000).
[4] D. Aoki, A. Huxley, E. Ressouche, D. Braithwaite, J. Flouquet, J. P. Brison, E. Lhotel, and C. Paulsen, Nature (London) **413**, 613 (2001).
[5] See, for instance D. Belitz, T. R. Kirkpatrick, and T. Vojta, Rev. Mod. Phys. **77**, 579 (2005); H. v. Lohneysen, A. Rosch, M. Vojta, and P. Wolfle, cond-mat/0606317 (to be published).
[6] D. T. Adroja, B. D. Rainford, S. K. Malik, M. Gailloux, and K. A. Gschneidner, Phys. Rev. B **50**, 248 (1994).
[7] P. Gegenwart, J. Custers, C. Geibel, K. Neumaier, T. Tayama, K. Tenya, O. Trovarelli, and F. Steglich, Phys. Rev. Lett. **89**, 056402 (2002).
[8] E. Morosan, S. L. Bud'ko, P. C. Canfield, M. S. Torikachvili, and A. H. Lacerda, J. Magn. Magn. Mater. **277**, 298 (2004).
[9] M. A. Avila, M. Sera, and T. Takabatake, Phys. Rev. B **70**, 100409(R) (2004).
[10] P. Bonville, P. Bellot, J. A. Hodges, P. Imbert, G. Jéhanno, G. Le Bras, J. Hammann, L. Leylekian, G. Chevrier, P. Thuéry, L. D'Onofrio, A. Hamzic, and A. Barthélémy, Physica B **182**, 105 (1992).
[11] K. Katoh, G. Terui, Y. Niide, S. Yoshii, K. Kindo, A. Oyamada, M. Shirikawa, and A. Ochiai, J. Alloys Compd. **360**, 225 (2003).
[12] Y. Muro, Y. Haizaki, M. S. Kim, K. Umeo, H. Tou, M. Sera, and T. Takabatake, Phys. Rev. B **69**, 020401(R) (2004).
[13] O. Trovarelli, C. Geibel, R. Cardoso, S. Mederle, R. Borth, B. Buschinger, F. M. Grosche, Y. Grin, G. Sparn, and F. Steglich, Phys. Rev. B **61**, 9467 (2000).
[14] J. L. Moriarity, J. E. Humphreys, R. O. Gordon, and N. C. Baenziger, Acta Crystallogr. **21**, 840 (1966).
[15] W. Bronger, J. Less-Common Met. **12**, 63 (1967).
[16] Q. Johnson, R. G. Bedford, and E. Catalano, J. Less-Common Met. **24**, 335 (1971).
[17] B. Erdmann and C. Keller, J. Solid State Chem. **7**, 40 (1973).
[18] A. Iandelli and A. Palenzona, J. Less-Common Met. **43**, 205 (1975).
[19] J. LeRoy, J-M. Moreau, D. Paccard, and E. Parthe, Acta Crystallogr., Sect. B: Struct. Crystallogr. Cryst. Chem. **B34**, 9 (1978).
[20] A. Iandelli and A. Palenzona, J. Less-Common Met. **80**, 71 (1981).
[21] F. Oster, B. Politt, E. Braunm, H. Schmidt, J. Langen, and N. Lossau, J. Magn. Magn. Mater. **63-64**, 629 (1987).
[22] H. Schmidt, B. Politt, F. Oster, and E. Braun, J. Less-Common Met. **134**, 187 (1987).
[23] P. Bonville, P. Imbert, G. Jehanno, F. Oster, and B. Politt, J. Phys.: Condens. Matter **2**, 4727 (1990).
[24] G. M. Sheldrick, SHELXL-97, Program for Crystal Structure Refinement, University of Göttingen, Germany, 1997.
[25] A. de Visser, J. J. M. Franse, and A. Menovsky, J. Magn. Magn. Mater. **43**, 43 (1984).
[26] V. T. Rajan, J. H. Lowenstein, and N. Andrei, Phys. Rev. Lett. **49**, 497 (1982).
[27] K. Kadowaki and S. B. Woods, Solid State Commun. **58**, 507 (1986).
[28] M. S. Kim, D. Sokolov, M. C. Bennett, M. C. Aronson, Q. Huang, Y. Chen, and J. W. Lynn (unpublished).